Langmuir

Article

pubs.acs.org/Langmuir

Opposing Effects of Humidity on Rhodochrosite Surface Oxidation

Chongzheng Na,*[,†,‡] Yuanzhi Tang,[‡,§] Haitao Wang,[†] and Scot T. Martin[‡]

[†]Department of Civil and Environmental Engineering and Earth Sciences, University of Notre Dame, 156 Fitzpatrick Hall, Notre Dame, Indiana 46556, United States

[‡]School of Engineering and Applied Sciences & Department of Earth and Planetary Sciences, Harvard University, 29 Oxford Street, Cambridge, Massachusetts 02138, United States

[§]School of Earth and Atmospheric Sciences, Georgia Institute of Technology, 311 Ferst Drive, Atlanta, Georgia 30332, United States

Supporting Information

ABSTRACT: Rhodochrosite ($MnCO_3$) is a model mineral representing carbonate aerosol particles containing redox-active elements that can influence particle surface reconstruction in humid air, thereby affecting the heterogeneous transformation of important atmospheric constituents such as nitric oxides, sulfur dioxides, and organic acids. Using in situ atomic force microscopy, we show that the surface reconstruction of rhodochrosite in humid oxygen leads to the formation and growth of oxide nanostructures. The oxidative reconstruction consists of two consecutive processes with distinctive time scales, including a long waiting period corresponding to slow nucleation and a rapid expansion phase corresponding to fast growth. By varying the relative humidity from 55 to 78%, we further show that increasing humidity has opposing effects on the two processes, accelerating nucleation from $2.8(\pm0.2) \times 10^{-3}$ to $3.0(\pm0.2) \times 10^{-2}$ h^{-1} but decelerating growth from $7.5(\pm0.3) \times 10^{-3}$ to $3.1(\pm0.1) \times 10^{-3}$ μm^2 h^{-1}. Through quantitative analysis, we propose that nanostructure nucleation is controlled by rhodochrosite surface dissolution, similar to the dissolution−precipitation mechanism proposed for carbonate mineral surface reconstruction in aqueous solution. To explain nanostructure growth in humid oxygen, a new Cabrera−Mott mechanism involving electron tunneling and solid-state diffusion is proposed.

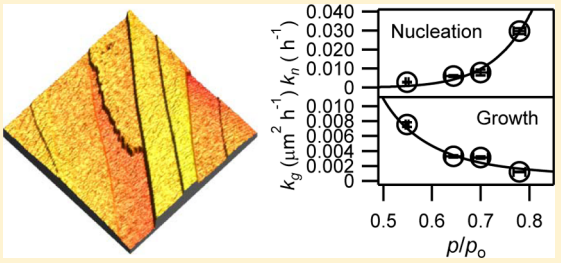

1. INTRODUCTION

Water vapor in the form of humidity is widely recognized as an important driver of mineral surface reconstruction in the atmosphere.[1] In humid air, water vapor condenses on mineral surfaces, creating a continuous layer of liquidlike water above a critical relative humidity (RH).[2] RH, a commonly used parameter for characterizing water vapor activity, is defined as the ratio of the partial pressure of water vapor to its saturated pressure at the same temperature (p/p_0). Although under ambient conditions the layer of condensed water is less than a few nanometers thick (nominal diameter of a water molecule: 0.34 nm),[3,4] it is surprisingly reactive with underlying carbonate minerals, a major component of aerosol dusts produced by winds blown over arid regions.[5,6] Observations made with atomic force microscopy (AFM) and related techniques show that water condensed on calcite ($CaCO_3$) can release mobile ions from the mineral surface through dissolution.[7] Extended exposure of calcite to humid air produces nanometer-thick surface islands, presumably through the precipitation of mobile ions, of hydrated calcite[8] or vaterite.[9] Further extension of exposure time leads to the growth of islands into continuous films.[9−12] AFM force measurements show that surface islands and films dominate the underlying carbonates in van der Waals and electrostatic interactions.[13−15] Given the generally recognized importance of carbonate mineral dusts in the atmosphere, these humidity-induced nanostructures can control the overall surface reactions between dust particles and atmospheric constituents such as nitric oxides,[16−24] sulfur dioxides,[17,24−27] and organic acids.[28−33]

Manganese (Mn), an important redox-active trace metal element in aerosol dusts, has been associated with calcite as a lattice impurity, which is often incorporated into calcite by substituting calcium.[34] A model structure of manganese carbonate is rhodochrosite ($MnCO_3$), which has the same rhombohedral structure as calcite.[35] Water is known to condense on the $(10\bar{1}4)$ surface of rhodochrosite in humid air, causing surface dissolution.[7,13,36] Different from calcite, however, the Mn^{2+} ions released from the dissolution of rhodochrosite can be oxidized by molecular oxygen in humid air to form surface oxide nanostructures.[37,38] The morphology, kinetics, and formation mechanism of Mn-containing nanostructures have not been investigated. A detailed understanding of these physicochemical parameters is crucial to assessing the influence of redox-active impurities such as manganese on atmospheric reactions involving aerosol dust particles.

Received: November 13, 2014
Revised: January 13, 2015
Published: February 5, 2015

DOI: 10.1021/la504465y
Langmuir 2015, 31, 2366−2371

2. EXPERIMENTAL SECTION

Natural rhodochrosite specimens were obtained from the Harvard Mineralogical Museum of Natural History. Pink translucent crystals with rhombohedral shapes were selected by visual inspection. Prior to each set of oxidation experiments, a fresh rhodochrosite surface was prepared by cleaving a crystal along the $(10\bar{1}4)$ plane of perfect cleavage. The cleaved crystal was then attached to a steel puck using warmed dental modeling wax (Cavex, Holland), with the fresh surface facing up.

The in situ investigation of nanostructure formation was performed using a custom-built AFM system consisting of a Veeco Multimode III microscope and an enclosing environmental chamber.[13] The chamber was supplied with humid O_2 and equipped with temperature and humidity sensors. The humidity in the chamber was controlled by altering the humidity of the supply gas, which was regulated by changing the fraction of dry gas passing through a piece of water-saturated Nafion tubing. The humidity control system was managed by a custom-written Igor (WaveMetrics, Lake Oswego, OR) routine using a proportional-integral-differential algorithm. Data acquisition and command delivery were executed using a PCI card (M6251, National Instruments, Austin, TX) and mass flow controllers (M100B, MKS Instruments, Andover, MA).

The formation of oxide films on a freshly cleaved rhodochrosite surface is monitored by periodically taking AFM images at a constant RH. Monitoring is performed using tapping mode over 100 μm × 100 μm randomly selected areas. The experimental temperature was stabilized around 25 °C, which was used to correct the reading of the humidity sensor in real time by the Igor routine.

3. RESULTS

Experiments performed to investigate rhodochrosite oxidation begin with cleaving a centimeter-sized rhodochrosite crystal with a razor blade.[13] As shown in Figure 1a, the surface of a freshly cleaved rhodochrosite $(10\bar{1}4)$ face consists of flat terraces separated by 0.26-nm-high atomic steps.[35] The steps extend in either the $[48\bar{1}]$ or $[\bar{4}41]$ direction,[35] forming long and narrow terrace lanes. The steps are not perfectly straight but smoothly curved, presumably reflecting the imperfect alignment of the razor blade with the $(10\bar{1}4)$ plane during cutting. The two steps confining a terrace lane extend in parallel until they eventually join each other, forming a terminal point (arrows in Figure 1a).

The exposure of rhodochrosite to humid O_2 induces the formation of thin films, sometimes with unclosed holes, on the $(10\bar{1}4)$ terraces, as shown by the AFM topography image in Figure 1b. Statistical analysis of a film inside a terrace lane (white box) reveals a topographical histogram that can be characterized by two Gaussian fits, as depicted in Figure 1c. The fit associated with lower topographical heights is attributed to the terrace whereas the fit with greater heights is attributed to the film. The difference in the two Gaussian means gives a film thickness of h = 1.0(±0.4) nm at 55% RH. As a control, when O_2 was replaced by high-purity N_2, no film was found within the same monitoring period.

Nanostructures formed on rhodochrosite by reacting with molecular oxygen have been previously identified as manganese oxides containing either Mn(III) or a mixture of Mn(II) and Mn(III).[38] The chemical and structural differences between the $MnCO_3$ substrate and overlying oxide film MnO_x ($1 < x < 2$) are evident in the AFM phase image of Figure 1d, which shows only two phases with merged step boundaries separating the same phase. The phase contrast is generated by differences between $MnCO_3$ and MnO_x in the surface-potential-dominated electrostatic interaction with the AFM tip.[13]

After more than 2 weeks of monitoring at 55% RH (monitoring frequency: at least once every 20 h), several nanometer-thick films are suddenly observed, as shown in Figure 2a, without any observation of scattered growth islands prior to the formation or during the growth of the films.

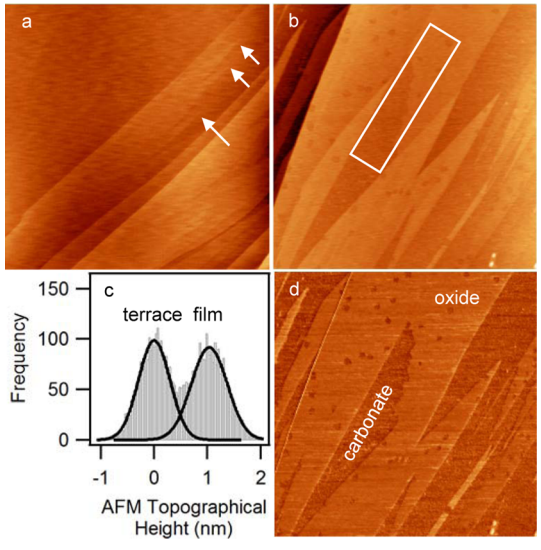

Figure 1. Formation of oxide films on rhodochrosite in humid air. (a) Freshly cleaved rhodochrosite surface (arrows: terminal points of terrace lanes). (b–d) Rhodochrosite exposed to O_2 at 55% relative humidity at around 25 °C: (b) atomic force microscopy (AFM) topography image, (c) histogram of the topographical height of the boxed area in b, and (d) AFM phase image. Size of a, b, and d: 10 μm × 10 μm.

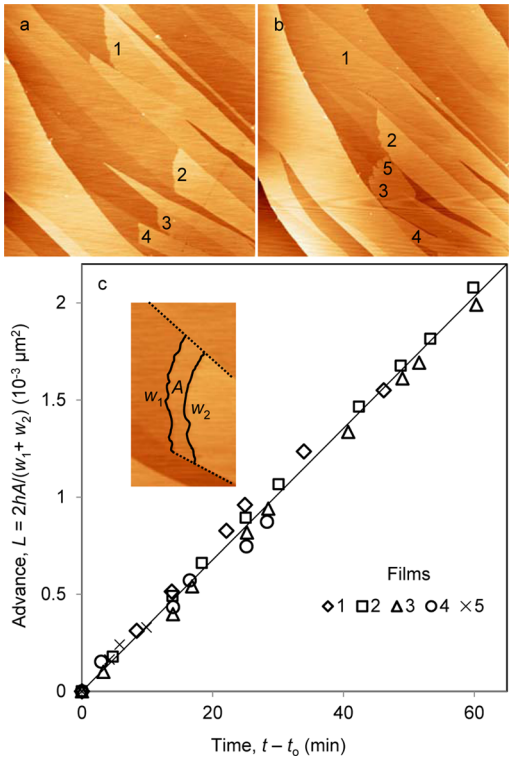

Figure 2. Kinetics of oxide film growth. (a, b) Films at t = 2040 and 2100 min. (c) Advance of the growth front with time. Image size: (a) 6.5 μm × 6.5 μm; (b) 9 μm × 9 μm. Film thickness: h = 1.0(±0.4) nm, as estimated from Figure 1c.

DOI: 10.1021/la504465y
Langmuir 2015, 31, 2366–2371

Besides the growth and extension of already-formed films, the formation of new films (e.g., Film 5 in Figure 2b) was also observed during continuous AFM monitoring, without the apparent formation of individual growth islands. This is different from observations made with calcite in humid air, which shows scattered islands and subsequent growth of the islands into films, suggesting that the nucleation and growth of nanostructures on calcite have comparable rates.[9−12] The lack of island formation on the rhodochrosite surface under our experimental conditions indicates that the nucleation and growth of manganese oxide films have dramatically different rates, with growth being much faster than nucleation. Indeed, the slow nucleation followed by rapid growth makes it impossible to capture the presence of nuclei under our experimental setup.

The time between the start of an experiment and the observation of the first growth film can be considered to be the time needed for heteroepitaxial nucleation, t_n, which is the reciprocal of the nucleation rate: $k_n = 1/t_n$. At 55% RH, t_n = 356(±20) h (longest time period elapsed between measurements in parentheses) and $k_n = 2.8(\pm 0.2) \times 10^{-3}$ h^{-1}. The formation of oxide films is not observed at RH below 55% with 2 weeks of monitoring. Variation of the AFM monitoring frequency does not promote nucleation, suggesting that nucleation is likely not influenced by AFM scanning. For RH greater than 55%, film formation is observed at shorter t_n and thus has faster k_n.

When oxide films are observed, most of them have already filled the width of the terrace lanes that they occupy (e.g., Films 1−4 in Figure 2a,b). The few still at the width-filling stage show that nucleation occurs at terrace steps (e.g., Film 5 in Figure 2b), consistent with previous observations of nanostructure nucleation on calcite[9−12] and presumably initiated at a kink site along the steps.[39] Once a film fills the width of the terrace lane, it advances rapidly with a rugged front (Movie S1). The advancement of the film eventually fills the entire terrace lane (e.g., Film 4 in Figure 2a,b).

The kinetics of film growth can be quantified by normalizing the advancement area A over the average length of growth fronts, $(w_1 + w_2)/2$, as shown by the inset of Figure 2c: $L = 2hA/(w_1 + w_2)$, where h is the film thickness. L estimated for different films shows a linear correlation with the growth time, $t - t_n$,

$$L = k_g(t - t_n) \quad (1)$$

where k_g is the growth rate and can be estimated from the slope of linearity. The conservation of k_g among films suggests that film growth is an autocatalyzed reaction, a well-known phenomenon for Mn^{2+} oxidation in solution.[40] The possibility that the movement of the AFM tip induces film growth is ruled out by varying the intervals between image scans and changing the scan direction (i.e., top down or bottom up). No tip influence is observed in our experiments, consistent with similar AFM measurements made with nanostructures grown on calcite.[10]

The three parameters used to characterizing rhodochrosite surface oxidation, namely, film thickness h, nucleation rate k_n, and growth rate k_g, are obtained under four different RH conditions, as shown in Figure 3. All three parameters show systematic correlations with RH, suggesting that rhodochrosite surface oxidation by molecular oxygen is regulated by humidity. As RH increases from 55 to 78%, h and k_n increase whereas k_g decreases, indicating opposing effects of humidity on nucleation and growth.

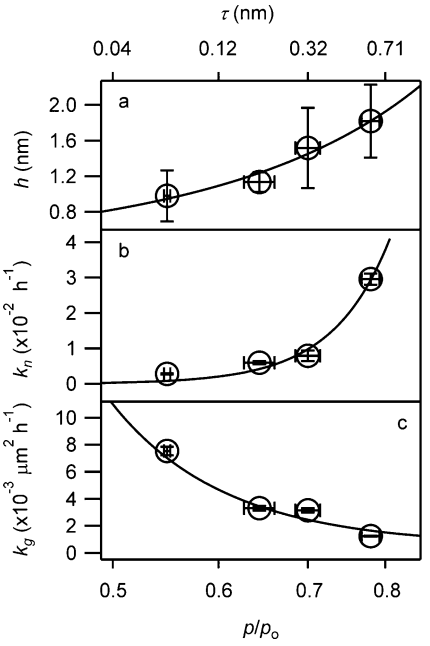

Figure 3. Dependence of (a) film thickness h, (b) nucleation rate k_n, and (c) growth rate k_g on relative humidity p/p_0. The condensed water thickness τ is estimated using the Freundlich isotherm constrained by water condensation on calcite at p/p_0 = 0 and 1 (Figure S1a). Curves in a, b, and c are least-squares regression to an exponential function, eq 2 or eq 3, respectively. The error bars in a are 1 standard deviation of the measured film thickness. The error bars in b are computed from the longest time period elapsed between measurements. The error bars in c are 68.3% confidence intervals obtained from the linear regression as illustrated in Figure 2c.

4. DISCUSSION

According to the experimental observations described above, we propose that the surface reconstruction of rhodochrosite in humid oxygen consists of two consecutive steps with distinctive time scales. As illustrated in Figure 4, the two steps are (a) nucleation initiated by the surface dissolution of $MnCO_3$, followed by the oxidation of released Mn^{2+}, and (b) the growth of Mn oxide films through autocatalytic oxidation regulated by oxygen dissolution in condensed water and the solid-state diffusion of Mn^{2+}. Details of the two-step mechanism, along

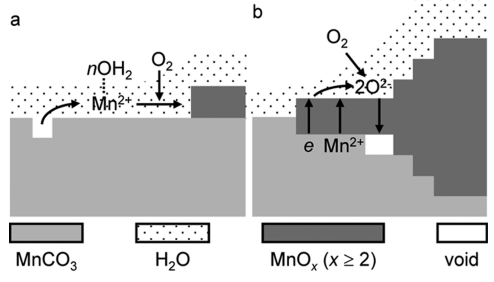

Figure 4. Schematics of rhodochrosite oxidation in humid oxygen: (a) nucleation initiated by surface dissolution, followed by oxidation and (b) growth through autocatalytic oxidation regulated by oxygen dissolution in condensed water and the solid-state diffusion of manganese. The release of CO_2 is not shown.

DOI: 10.1021/la504465y
Langmuir 2015, 31, 2366−2371

with the quantitative account of the relationships of h, k_n, and k_g with RH, are described as follows.

The dependence of h on RH (Figure 3a) is similar to the dependence of condensed water thickness τ on RH.[3,4] According to water condensation on calcite (Figure S1a),[3] $\tau = 2.7(p/p_0)^a$ in nanometers (see below for the estimation of a), following the Freundlich isotherm[41] with limiting conditions of $\tau = 0$ at $p/p_0 = 0$ and $\tau = 2.7$ nm at $p/p_0 = 1$. In comparison, h is approximately 1 nm higher than τ (Figure S1b) but lower than the self-limiting thickness of 2.3−2.5 nm suggested for MnO_x films in aqueous solutions.[38] The correlation of h and τ (Figure S1b) suggests that the nucleation of oxide nanostructures begins with $MnCO_3$ dissolving in water condensed on rhodochrosite from the vapor phase, which generates Mn^{2+}.[42,43]

Dissolved Mn^{2+} on the rhodochrosite surface is then oxidized by molecular oxygen dissolved in the condensed water layer. Although the homogeneous oxidation of Mn^{2+} by O_2 is slow, the presence of a surface such as rhodochrosite can greatly accelerate the reaction.[44] The presence of a stabilizing surface presumably improves the rate of ligand exchange with oxygen, leading to the inner-sphere oxidation of manganese.[45] In addition, the surface can also stabilize oxidation product MnO_x by providing anions and water for coordination.

The oxidation of surface Mn^{2+} can provide a sufficient number of MnO_x monomers for film nucleation. Using the solubility of bulk rhodochrosite in the aqueous solution ($pK_{sp} = -4.4$),[46] we estimate that the surface density of Mn^{2+} is 1.9×10^{15} ions m^{-2} by assuming $[Mn^{2+}] = [CO_3^{2-}]$. This is obviously an underestimate because CO_3^{2-} should have a much lower concentration due to the escape of CO_2 gas (no CO_2 in the influx of oxygen). Even with the underestimated surface density, 19 000 Mn^{2+} ions are present on a streak of a 1 μm × 10 μm terrace, which is a significant number for surface nucleation. Even if only a small fraction (e.g., 1%) of Mn^{2+} is involved in forming a two-dimensional nucleus with a height of 1 nm, the nucleus could be as large as 1.25 nm in diameter (molecular volumes of $MnCO_3$ and $^1/_2(Mn_2O_3)$: 51 and 26 Å^3),[35,47] comparable to the expected critical size of carbonate nuclei.[48]

As shown in Figure 3a, k_n increases with increasing RH, ranging from $2.8(\pm0.2) \times 10^{-3}$ h^{-1} at 55% RH to $3.0(\pm0.2) \times 10^{-2}$ h^{-1} at 78% RH (corresponding to $t_n = 34(\pm2)$ and 356(±20) h, respectively). In comparison, the nucleation of oxide nanostructures on rhodochrosite takes less than 5 h in the O_2-saturated aqueous solution, corresponding to $k_n > 0.2$ h^{-1}.[38] The slower nucleation kinetics in humid oxygen can be attributed to the slow kinetics of Mn^{2+} dissolution to achieve supersaturation. Compared to manganese dissolution in the aqueous solution, dissolution in humid oxygen is limited by the availability of water molecules. For the successful dissolution of surface-bound Mn(II) atoms, the positive charges of the cation must be screened rather than being exposed directly to the gas phase. Screening is provided by coordination with n water molecules, reducing the total free energy regulated by the water vapor pressure: $\Delta G = \Delta G_0 - nRT \ln(p/p_0)$, where ΔG_0 is the change in free energy with saturated water vapor, $R = 8.314$ J K^{-1} mol^{-1} is the gas constant, and $T = 298$ K is the absolute temperature. Hence, for manganese dissolution in humid oxygen with hydration as the rate-limiting step, we can expect

$$k_n = k_{n,o} \exp\left(-\frac{\Delta G}{RT}\right) = k_{n,o} \exp\left(-\frac{\Delta G_o}{RT} + n \ln \frac{p}{p_0}\right) \quad (2)$$

where $k_{n,o}$ is the rate at $\Delta G = 0$. Using the data in Figure 3b, we estimate $n = 10(\pm4)$ through least-squares regression ($R^2 = 0.97$). The value of n is consistent with the number of water molecules needed to coordinate a divalent cation with two hydration layers (first layer, 6; second layer, 12) in a half-sphere configuration (half of ca. 18 water molecules).[49] ΔG_0 and $k_{n,o}$ are estimated to be on the orders of 2.5 kJ mol^{-1} and 1 h^{-1}, consistent with the Gibbs free energy and kinetics associated with carbonate dissolution.[50,51]

Of note, it is unlikely that the oxidation of Mn^{2+} and the formation of the MnO_x nucleus have played significant roles in regulating nucleation kinetics. The inner-sphere oxidation of Mn^{2+} requires that oxygen penetrates the coordination shells of water,[45] which is expected not to vary with RH because the shell thickness is constant (i.e., two hydration layers as suggested by $n = 10$). The nucleation of MnO_x monomers requires desolvation,[39] which is increasingly difficult with increasing RH and would have led to the decrease in k_n.

Once a nucleus is formed, it grows rapidly through the autocatalytic oxidation of Mn^{2+} at the edge of the nucleus. Measurements of k_g in humid O_2 are comparable to those in the aqueous solution equilibrated with 1 atm of O_2.[38] The decrease in k_g with increasing RH, however, suggests that film growth is not a surface-controlled reaction, which would have led to a constant k_g across the experimental RH range. Instead, we propose that film growth in humid O_2 is controlled by the diffusion of oxygen through the water layer condensed on rhodochrosite. According to Fick's law, the flux of diffusion is $J = -D(dC/d\tau) \approx DP/(H\tau)$, where D is the diffusion coefficient, $P = 1$ atm is the oxygen pressure, and $H = 769$ atm L mol^{-1} is Henry's constant for oxygen dissolution at 25 °C. Taking into consideration condensed water thickness τ and oxide film thickness h, the growth rate is thus expected to be

$$k_g = J\upsilon h \approx \frac{DP\upsilon h}{H\tau} \quad (3)$$

where $\upsilon = 10^{-5}$ m^3 mol^{-1} is the molar volume of $^2/_3(Mn_2O_3)$.[47] With $\tau = 2.7(p/p_0)^a$, the least-squares regression of eq 3 to data presented in Figure 3c gives $D = 1.2(\pm0.3) \times 10^{-11}$ m^2 s^{-1} and $a = 6.0(\pm0.4)$ ($R^2 = 0.95$). The value of D is smaller than not only the gas-phase diffusivity of 2×10^{-5} m^2 s^{-1} for O_2 but also its aqueous-phase diffusivity of 2×10^{-9} m^2 s^{-1},[52] suggesting that the condensed water on rhodochrosite acts like a solid phase. This is consistent with the proposal that the first layer of condensed water on a mineral surface is icelike.[2,53,54]

In addition to the diffusion-limited supply of oxygen, the supply of manganese is also limited for rhodochrosite in contact with humid gas. When rhodochrosite is placed in an aqueous solution, the solution serves as a large reservoir of Mn^{2+}. Manganese consumed by oxidation can be replenished by dissolution from the surface areas that are not covered by nanostructures,[38] with the solution serving as a conduit channeling Mn^{2+} from dissolution sites to growth sites. In humid O_2, a terrace lane supporting the growth of a film is confined by two semiparallel steps, which confine the diffusion of Mn^{2+} ions within the thin layer of condensed water and inhibit the supply of Mn^{2+} from outside the lane by forming Ehrlich−Schwoebel barriers.[55] In spite of the spatial confinement, films can grow into the terminal ends of terrace lanes without a discernible reduction in growth rate or film thickness (e.g., Films 1 and 4 in Figure 2). This calls into question the supply of Mn^{2+} by dissolution and lateral diffusion, which would suggest the deceleration of growth, thinning of films, and

DOI: 10.1021/la504465y
Langmuir 2015, 31, 2366−2371

formation and deepening of dissolution pits as growth approaches terminal ends.

So what is the mass-transfer pathway for manganese to supply film growth? We propose that the diffusion of manganese follows a Cabrera−Mott mechanism that is widely used to describe metal oxidation.[56] This mechanism consists of several steps. First, electrons tunnel through the first layer of the semiconducting film, which is formed by the catalytic oxidation of surface Mn^{2+} at the edge of a nucleus.[57] Second, electron reduces oxygen and forms oxygen ions on top of the film layer. Upon completion of these steps, an electrical field is established by the positively charged holes left behind by electron tunneling and the negatively charged surface oxygen. This leads to the third step, which is the counter diffusion of Mn^{2+} and O^{2-} under the electrical field. For the oxidation of iron to γ-Fe_2O_3, the Cabrera−Mott diffusion is almost instantaneous for films that are less than 1 nm thick but diminishes to a virtual stop for films thicker than 2 nm.[58] This is consistent with the self-limited heights of 1 to 2 nm observed for manganese oxide films over rhodochrosite. Certainly, the confirmation of the proposed mechanism requires direct experimental evidence in future studies.

5. SUMMARY

We have quantified the kinetics of nanostructure formation on a rhodochrosite surface in humid oxygen using in situ AFM. The formation of oxide nanostructures on rhodochrosite consists of a long waiting period before the presence of nanostructures, followed by a rapid advance of growth fronts. We interpret the long wait as slow oxide nucleation and the rapid advance as fast growth. By varying the relative humidity and thus the amount of condensed water on the rhodochrosite surface, we find that the slow nucleation is controlled by $MnCO_3$ dissolution whereas the rapid growth is limited by oxygen diffusion. We propose that the nucleation of oxide nanostructures follows a dissolution−precipitation mechanism similar to that in aqueous solution. The growth of oxide films, however, conforms to a Cabrera−Mott mechanism involving electron tunneling and solid-state diffusion. The complex mechanism revealed here suggests that the presence of redox-active elements in aerosol dust particles can greatly complicate the transformation of these particles in a humid atmosphere.

■ ASSOCIATED CONTENT

Supporting Information

Figure S1: The thickness of water condensed on calcite in humid air and its correlation with the thickness of the oxide film formed on rhodochrosite. Movie S1: Advancement of oxide films with time. This material is available free of charge via the Internet at http://pubs.acs.org.

■ AUTHOR INFORMATION

Corresponding Author

*E-mail: chongzheng.na@gmail.com.

Notes

The authors declare no competing financial interest.

■ ACKNOWLEDGMENTS

C.N. thanks the National Science Foundation Environmental Engineering Program, the donors of the American Chemical Society Petroleum Research Fund (ACS-PRF), and the Notre Dame Sustainable Energy Initiative for financial support. Y.T. acknowledges support from ACS-PRF and the Georgia Institute of Technology.

■ REFERENCES

(1) Rubasinghege, G.; Grassian, V. H. Role(s) of adsorbed water in the surface chemistry of environmental interfaces. *Chem. Commun.* **2013**, *49*, 3071−3094.

(2) Hu, J.; Xiao, X.-D.; Ogletree, D. F.; Salmeron, M. Imaging the condensation and evaporation of molecularly thin films of water with nanometer resolution. *Science* **1995**, *268*, 267−269.

(3) Gustafsson, R. J.; Orlov, A.; Badger, C. L.; Griffiths, P. T.; Cox, R. A.; Lambert, R. M. A comprehensive evaluation of water uptake on atmospherically relevant mineral surfaces: DRIFT spectroscopy, thermogravimetric analysis and aerosol growth measurements. *Atmos. Chem. Phys.* **2005**, *5*, 3415−3421.

(4) Rahaman, A.; Grassian, V. H.; Margulis, C. J. Dynamics of water adsorption onto a calcite surface as a function of relative humidity. *J. Phys. Chem. C* **2008**, *112*, 2109−2115.

(5) Husar, R. B.; Tratt, D. M.; Schichtel, B. A.; Falke, S. R.; Li, F.; Jaffe, D.; Gasso, S.; Gill, T.; Laulainen, N. S.; Lu, F.; Reheis, M. C.; Chun, Y.; Westphal, D.; Holben, B. N.; Gueymard, C.; McKendry, I.; Kuring, N.; Feldman, G. C.; McClain, C.; Frouin, R. J.; Merrill, J.; DuBois, D.; Vignola, F.; Murayama, T.; Nickovic, S.; Wilson, W. E.; Sassen, K.; Sugimoto, N.; Malm, W. C. Asian dust events of April 1998. *J. Geophys. Res. Atmos.* **2001**, *106*, 18317−18330.

(6) Bauer, S. E.; Balkanski, Y.; Schulz, M.; Hauglustaine, D. A.; Dentener, F. Global modeling of heterogeneous chemistry on mineral aerosol surfaces: Influence on tropospheric ozone chemistry and comparison to observations. *J. Geophys. Res. Atmos.* **2004**, *109*, D02304.

(7) Kendall, T. A.; Martin, S. T. Mobile ions on carbonate surfaces. *Geochim. Cosmochim. Acta* **2005**, *69*, 3257−3263.

(8) Kendall, T. A.; Martin, S. T. Water-induced reconstruction that affects mobile ions on the surface of calcite. *J. Phys. Chem. A* **2007**, *111*, 505−514.

(9) Baltrusaitis, J.; Grassian, V. H. Calcite surface in humid environments. *Surf. Sci.* **2009**, *603*, L99−L104.

(10) Stipp, S. L. S.; Gutmannsbauer, W.; Lehmann, T. The dynamic nature of calcite surfaces in air. *Am. Mineral.* **1996**, *81*, 1−8.

(11) Kendall, T. A.; Martin, S. T. Water-induced reconstruction that affects mobile ions on the surface of calcite. *J. Phys. Chem. A* **2006**, *111*, 505−514.

(12) Hausner, D. B.; Reeder, R. J.; Strongin, D. R. Humidity-induced restructuring of the calcite surface and the effect of divalent heavy metals. *J. Colloid Interface Sci.* **2007**, *305*, 101−110.

(13) Na, C.; Kendall, T. A.; Martin, S. T. Surface-potential heterogeneity of reacted calcite and rhodochrosite. *Environ. Sci. Technol.* **2007**, *41*, 6491−6497.

(14) Na, C.; Martin, S. T. Interfacial forces are modified by the growth of surface nanostructures. *Environ. Sci. Technol.* **2008**, *42*, 6883−6889.

(15) Na, C.; Martin, S. T. Growth of manganese oxide nanostructures alters the layout of adhesion on a carbonate substrate. *Environ. Sci. Technol.* **2009**, *43*, 4967−4972.

(16) Al-Abadleh, H. A.; Krueger, B. J.; Ross, J. L.; Grassian, V. H. Phase transitions in calcium nitrate thin films. *Chem. Commun.* **2003**, *22*, 2796−2797.

(17) Al-Hosney, H. A.; Grassian, V. H. Water, sulfur dioxide and nitric acid adsorption on calcium carbonate: A transmission and ATR-FTIR study. *Phys. Chem. Chem. Phys.* **2005**, *7*, 1266−1276.

(18) Krueger, B. J.; Ross, J. L.; Grassian, V. H. Formation of microcrystals, micropuddles, and other spatial inhomogenieties in surface reactions under ambient conditions: An atomic force microscopy study of water and nitric acid adsorption on MgO(100) and $CaCO_3$(1014). *Langmuir* **2005**, *21*, 8793−8801.

(19) Prince, A. P.; Grassian, V. H.; Kleiber, P.; Young, M. A. Heterogeneous conversion of calcite aerosol by nitric acid. *Phys. Chem. Chem. Phys.* **2007**, *9*, 622−634.

DOI: 10.1021/la504465y
Langmuir 2015, 31, 2366−2371

(20) Liu, Y.; Gibson, C.; Wang, H.; Grassian; Laskin, A. Kinetics of heterogeneous reaction of $CaCO_3$ particles with gaseous HNO_3 over a wide range of humidity. *J. Phys. Chem. A* **2008**, *112*, 1561−1571.
(21) Li, H. J.; Zhu, T.; Zhao, D. F.; Zhang, Z. F.; Chen, Z. M. Kinetics and mechanisms of heterogeneous reaction of NO_2 on $CaCO_3$ surfaces under dry and wet conditions. *Atmos. Chem. Phys.* **2010**, *10*, 463−474.
(22) Baltrusaitis, J.; Grassian, V. H. Atomic force microscopy and X-ray photoelectron spectroscopy study of NO_2 reactions on $CaCO_3$ (10(1)bar4) surfaces in humid environments. *J. Phys. Chem. A* **2012**, *116*, 9001−9009.
(23) Zhao, Y.; Chen, Z.; Shen, X.; Huang, D. Heterogeneous reactions of gaseous hydrogen peroxide on pristine and acidic gas-processed calcium carbonate particles: Effects of relative humidity and surface coverage of coating. *Atmos. Environ.* **2013**, *67*, 63−72.
(24) Al-Hosney, H. A.; Grassian, V. H. Carbonic acid: An important intermediate in the surface chemistry of calcium carbonate. *J. Am. Chem. Soc.* **2004**, *126*, 8068−8069.
(25) Li, L.; Chen, Z. M.; Zhang, Y. H.; Zhu, T.; Li, J. L.; Ding, J. Kinetics and mechanism of heterogeneous oxidation of sulfur dioxide by ozone on surface of calcium carbonate. *Atmos. Chem. Phys.* **2006**, *6*, 2453−2464.
(26) Baltrusaitis, J.; Usher, C. R.; Grassian, V. H. Reactions of sulfur dioxide on calcium carbonate single crystal and particle surfaces at the adsorbed water carbonate interface. *Phys. Chem. Chem. Phys.* **2007**, *9*, 3011−3024.
(27) Prince, A. P.; Kleiber, P.; Grassian, V. H.; Young, M. A. Heterogeneous interactions of calcite aerosol with sulfur dioxide and sulfur dioxide-nitric acid mixtures. *Phys. Chem. Chem. Phys.* **2007**, *9*, 3432−3439.
(28) Al-Hosney, H. A.; Carlos-Cuellar, S.; Baltrusaitis, J.; Grassian, V. H. Heterogeneous uptake and reactivity of formic acid on calcium carbonate particles: a Knudsen cell reactor, FTIR and SEM study. *Phys. Chem. Chem. Phys.* **2005**, *7*, 3587−3595.
(29) Usher, C. R.; Baltrusaitis, J.; Grassian, V. H. Spatially resolved product formation in the reaction of formic acid with calcium carbonate (10(-1)4): The role of step density and adsorbed water-assisted ion mobility. *Langmuir* **2007**, *23*, 7039−7045.
(30) Prince, A. P.; Kleiber, P. D.; Grassian, V. H.; Young, M. A. Reactive uptake of acetic acid on calcite and nitric acid reacted calcite aerosol in an environmental reaction chamber. *Phys. Chem. Chem. Phys.* **2008**, *10*, 142−152.
(31) Ma, Q.; Liu, Y.; Liu, C.; He, H. Heterogeneous reaction of acetic acid on MgO, α-Al_2O_3, and $CaCO_3$ and the effect on the hygroscopic behaviour of these particles. *Phys. Chem. Chem. Phys.* **2012**, *14*, 8403−8409.
(32) Karoussi, O.; Skovbjerg, L. L.; Hassenkam, T.; Stipp, S. L. S.; Hamouda, A. A. AFM study of calcite surface exposed to stearic and heptanoic acids. *Colloids Surf., A* **2008**, *325*, 107−114.
(33) Cooke, D. J.; Gray, R. J.; Sand, K. K.; Stipp, S. L. S.; Elliott, J. A. Interaction of ethanol and water with the {10(-1)4} surface of calcite. *Langmuir* **2010**, *26*, 14520−14529.
(34) Aghnatios, C.; Losno, R.; Dulac, F. A fine fraction of soil used as an aerosol analogue during the DUNE experiment: sequential solubility in water with step-by-step decreasing pH. *Biogeosci. Discuss.* **2014**, *11*, 2623−2637.
(35) Maslen, E. N.; Streltsov, V. A.; Streltsova, N. R.; Ishizawa, N. Electron density and optical anisotropy in rhombohedral carbonates. 3. Synchrotron x-ray studies of $CaCO_3$, $MgCO_3$ and $MnCO_3$. *Acta Crystallogr., Sect. B* **1995**, *51*, 929−939.
(36) Kendall, T. A.; Na, C.; Jun, Y.-S.; Martin, S. T. Electrical properties of mineral surfaces for increasing water sorption. *Langmuir* **2008**, *24*, 2519−2524.
(37) Duckworth, O. W.; Martin, S. T. Role of molecular oxygen in the dissolution of siderite and rhodochrosite. *Geochim. Cosmochim. Acta* **2004**, *68*, 607−621.
(38) Jun, Y. S.; Kendall, T. A.; Martin, S. T.; Friend, C. M.; Vlassak, J. J. Heteroepitaxial nucleation and oriented growth of manganese oxide islands on carbonate minerals under aqueous conditions. *Environ. Sci. Technol.* **2005**, *39*, 1239−1249.
(39) Markov, I. *Crystal Growth for Beginners: Fundamentals of Nucleation, Crystal Growth and Epitaxy*; World Scientific Publishing: River Edge, NJ, 1995.
(40) Kessick, M. A.; Morgan, J. J. Mechanism of autoxidaton of manganese in aqueous solution. *Environ. Sci. Technol.* **1975**, *9*, 157−159.
(41) Hatch, C. D.; Wiese, J. S.; Crane, C. C.; Harris, K. J.; Kloss, H. G.; Baltrusaitis, J. Water adsorption on clay minerals as a function of relative humidity: Application of BET and Freundlich adsorption models. *Langmuir* **2011**, *28*, 1790−1803.
(42) Dai, Q.; Hu, J.; Salmeron, M. Adsorption of water on NaCl (100) surfaces: Role of atomic steps. *J. Phys. Chem. B* **1997**, *101*, 1994−1998.
(43) Luna, M.; Rieutord, F.; Melman, N. A.; Dai, Q.; Salmeron, M. Adsorption of water on alkali halide surfaces studied by scanning polarization force microscopy. *J. Phys. Chem. A* **1998**, *102*, 6793−6800.
(44) Morgan, J. J. Kinetics of reaction between O_2 and Mn(II) species in aqueous solutions. *Geochim. Cosmochim. Acta* **2005**, *69*, 35−48.
(45) Rosso, K. M.; Morgan, J. J. Outer-sphere electron transfer kinetics of metal ion oxidation by molecular oxygen. *Geochim. Cosmochim. Acta* **2002**, *66*, 4223−4233.
(46) Langmuir, D. Techniques of Estimating Thermodynamic Properties for Some Aqueous Complexes of Geochemical Interest. In *Chemical Modeling in Aqueous Systems*; American Chemical Society: Washington, DC, 1979; Vol. *93*, pp 353−387.
(47) Geller, S. Structures of α-Mn_2O_3, $(Mn_{0.983}Fe_{0.017})_2O_3$ and $(Mn_{0.37}Fe_{0.63})_2O_3$ and relation to magnetic ordering. *Acta Crystallogr., Sect. B* **1971**, *27*, 821.
(48) Pouget, E. M.; Bomans, P. H. H.; Goos, J. A. C. M.; Frederik, P. M.; de With, G.; Sommerdijk, N. A. J. M. The initial stages of template-controlled $CaCO_3$ formation revealed by cryo-TEM. *Science* **2009**, *323*, 1455−1458.
(49) Bol, W.; Gerrits, G. J. A.; van Panthaleon Eck, C. L. The hydration of divalent cations in aqueous solution. An X-ray investigation with isomorphous replacement. *J. Appl. Crystallogr.* **1970**, *3*, 486−492.
(50) Xu, J.; Fan, C.; Teng, H. H. Calcite dissolution kinetics in view of Gibbs free energy, dislocation density, and pCO_2. *Chem. Geol.* **2012**, *322*−*323*, 11−18.
(51) Duckworth, O. W.; Cygan, R. T.; Martin, S. T. Linear free energy relationships between dissolution rates and molecular modeling energies of rhombohedral carbonates. *Langmuir* **2004**, *20*, 2938−2946.
(52) Han, P.; Bartels, D. M. Temperature dependence of oxygen diffusion in H_2O and D_2O. *J. Phys. Chem.* **1996**, *100*, 5597−5602.
(53) Fenter, P.; Sturchio, N. C. Calcite (104)−water interface structure, revisited. *Geochim. Cosmochim. Acta* **2012**, *97*, 58−69.
(54) Fenter, P.; Kerisit, S.; Raiteri, P.; Gale, J. D. Is the calcite−water interface understood? Direct comparisons of molecular dynamics simulations with specular X-ray reflectivity data. *J. Phys. Chem. C* **2013**, *117*, 5028−5042.
(55) Lagally, M. G.; Zhang, Z. Thin-film cliffhanger. *Nature* **2002**, *417*, 907−910.
(56) Cabrera, N.; Mott, N. F. Theory of the oxidation of metals. *Rep. Prog. Phys.* **1948**, *12*, 163−184.
(57) Preisler, E. Semiconductor properties of manganese dioxide. *J. Appl. Electrochem.* **1976**, *6*, 311−320.
(58) Fung, K. K.; Qin, B.; Zhang, X. X. Passivation of α-Fe nanoparticle by epitaxial γ-Fe_2O_3 shell. *Mater. Sci. Eng., A* **2000**, *286*, 135−138.

DOI: 10.1021/la504465y
Langmuir 2015, 31, 2366−2371